LETTERS

Common effector processing mediates cell-specific responses to stimuli

Kathryn Miller-Jensen[1,2]*, Kevin A. Janes[1,3]*, Joan S. Brugge[3] & Douglas A. Lauffenburger[1,2,4]

The fundamental components of many signalling pathways are common to all cells[1–3]. However, stimulating or perturbing the intracellular network often causes distinct phenotypes that are specific to a given cell type[4,5]. This 'cell specificity' presents a challenge in understanding how intracellular networks regulate cell behaviour and an obstacle to developing drugs that treat signalling dysfunctions[6,7]. Here we apply a systems-modelling approach[8] to investigate how cell-specific signalling events are integrated through effector proteins to cause cell-specific outcomes. We focus on the synergy between tumour necrosis factor and an adenoviral vector as a therapeutically relevant stimulus that induces cell-specific responses[9–11]. By constructing models that estimate how kinase-signalling events are processed into phenotypes through effector substrates, we find that accurate predictions of cell specificity are possible when different cell types share a common 'effector-processing' mechanism. Partial-least-squares regression models based on common effector processing accurately predict cell-specific apoptosis, chemokine release, gene induction, and drug sensitivity across divergent epithelial cell lines. We conclude that cell specificity originates from the differential activation of kinases and other upstream transducers, which together enable different cell types to use common effectors to generate diverse outcomes. The common processing of network signals by downstream effectors points towards an important cell biological principle, which can be applied to the understanding of cell-specific responses to targeted drug therapies[6].

Signalling networks arise from complex modular interactions among the adaptors, enzymes, and other transducer proteins that together transmit information[12] (Fig. 1a). Experimental[13] and literature-based[14] reconstructions of signalling networks often assume that there exists a common network whose connectivity is the same for all cells[15]. However, cellular responses to stimuli are usually specific to a given cell type. How are cell-specific responses achieved through a common signalling network? To answer this question, it is important to consider the downstream effector substrates (including cytoplasmic targets, transcription factors and terminal enzymes) that ultimately 'process' the activation of transducer proteins into cell-specific phenotypes (Fig. 1a).

We investigated how effector substrates process signalling-network information by using a defined experimental setup with clear, cell-specific outcomes. Adenoviral gene-therapy vectors (Adv) synergize with the cytokine tumour necrosis factor (TNF) in many cellular contexts[11,16,17]. The binding and entry of Adv activates many pathways that are shared with TNF (Supplementary Table 1). In epithelial cells, apoptosis caused by the synergistic combination of Adv and TNF occurs together with Adv-induced changes in activation of the TNF signalling network[11]. Interestingly, the extent
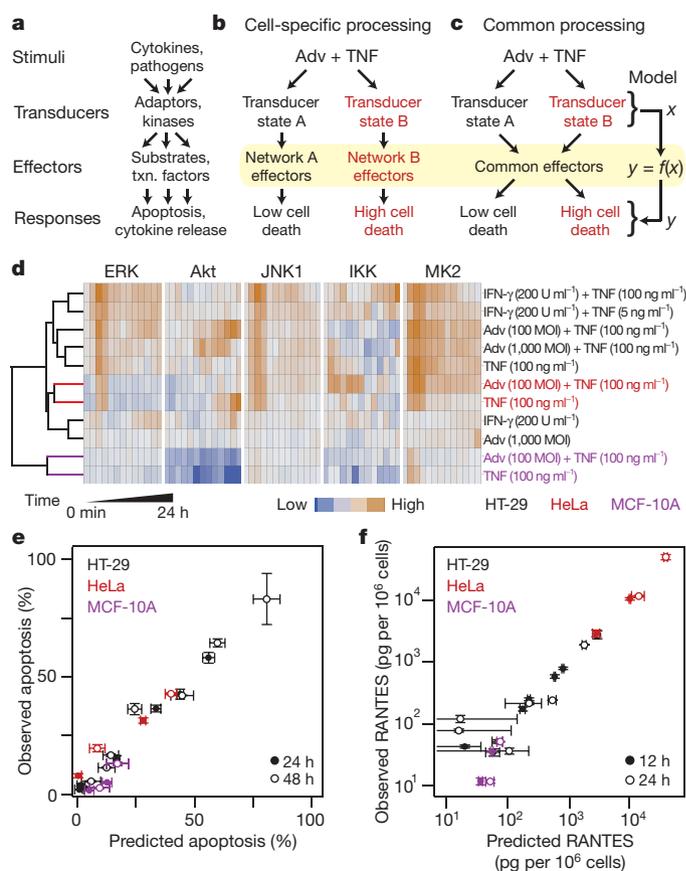

Figure 1 | Test of a common effector-processing hypothesis in epithelial cells treated with Adv plus TNF. a, Flow of information from stimuli through transducers and effectors to responses. Txn factors, transcription factors. **b**, **c**, Cell-specific (**b**) and common effector-processing mechanisms (**c**) linking treatment with Adv plus TNF to apoptosis. A model of effector processing, $f(x)$, links transducer activation to responses. **d**, Time-dependent kinase activities in HT-29 (black), HeLa (red) and MCF-10A (purple) cells treated with different combinations of Adv, IFN-γ and TNF[18,19]. Data are presented as the mean of duplicate (Adv) or triplicate (IFN-γ) biological samples (see Methods and Supplementary Table 5 for details). MOI, multiplicity of infection. **e**, **f**, Correlation between predictions of the common-processing model and measurements of apoptosis (**e**) or RANTES secretion (**f**). Model training with HT-29 cells (black) is compared to model predictions of HeLa (red) and MCF-10A (purple) cells at 24 h (filled) and 48 h (open) after treatment for apoptosis or 12 h (filled) and 24 h (open) after treatment for RANTES secretion. Experimental data are presented as the mean ± s.e. ($n = 3$), and model uncertainties are estimated by jack-knifing[30].

[1]Center for Cell Decision Processes, Massachusetts Institute of Technology, Cambridge, Massachusetts 02139, USA. [2]Department of Chemical Engineering, Massachusetts Institute of Technology, Cambridge, Massachusetts 02139, USA. [3]Department of Cell Biology, Harvard Medical School, Boston, Massachusetts 02115, USA. [4]Departments of Biology and Biological Engineering, Massachusetts Institute of Technology, Cambridge, Massachusetts 02139, USA.
*These authors contributed equally to this work.

of Adv–TNF synergy is specific to cell type: HeLa cervical carcinoma cells are much more sensitive to apoptosis than HT-29 colon adeno-carcinoma cells when pre-infected with the same virus-to-cell ratio and stimulated with the same concentration of TNF[11] (Supplementary Fig. 1a, b).

There are two possible mechanisms by which cell-specific outcomes to a stimulus might be mediated. First, both the level of signal activation and the mechanism of effector processing could be cell specific (Fig. 1b). In this scenario, a given signalling event (for instance, the activation of a protein kinase) would contribute differently to a phenotype, depending on the particular cell type in which the signal was activated. A simpler alternative is that signal activation is sufficient to confer cell-specific outcomes (Fig. 1c). In this case, the main determinant of cell specificity would be the strength and combination of activation events induced by the stimulus. Different cell types could then use a common effector-processing mechanism that integrates these cell-specific signalling events to elicit cell-specific responses. Typically, the molecular details that link transducers to effectors and responses are incompletely understood. We therefore tested these two hypotheses by measuring the intracellular network and then mathematically calculating the bulk contribution of transducer proteins to effector processing (Fig. 1c; $f(x)$).

We selected an Adv–TNF treatment that causes a several-fold greater apoptotic response in HeLa cells than in HT-29 cells (Supplementary Fig. 1a–d). To monitor network activation induced by treatment with Adv and TNF, we measured the activities of five kinases that are important in Adv–TNF signalling and apoptosis: extracellular signal-regulated kinase (ERK), the serine-threonine protein kinase B (PKB)/Akt, c-Jun N-terminal kinase 1 (JNK1), inhibitor of nuclear factor (NF)-κB kinase (IKK), and MAPK-activated protein kinase 2 (MK2) (Supplementary Table 1). We observed significant differences in the dynamic activation of Akt, JNK1, IKK and MK2 between uninfected and Adv-infected HeLa cells that were stimulated with TNF ($P < 0.01$; Supplementary Fig. 2a), confirming that Adv had perturbed kinase signalling en route to apoptosis. Importantly, there were also significant differences in the dynamics of ERK, Akt, JNK1 and IKK activation between Adv-infected HT-29 cells and Adv-infected HeLa cells ($P < 0.001$; Supplementary Fig. 2b). Therefore, Adv infection perturbs the TNF-activated kinase network in epithelial cells[11] and the nature of the perturbation is cell specific.

Interferon-γ (IFN-γ) also sensitizes TNF-induced apoptosis and converges upon many of the same pathways as TNF and Adv[11,18]. Therefore, we compared the cell-specific activity measurements with published time courses of signalling induced by IFN-γ and TNF in HT-29 cells[18,19] (Fig. 1d). Hierarchical clustering of the concatenated kinase-activity time courses indicated that the HeLa cell signalling profiles, although different from HT-29 profiles for the same stimulus, were roughly similar to network states that could be achieved by HT-29 cells.

Because the signalling dynamics of HeLa and HT-29 cells were homologous overall (Fig. 1d) but their apoptotic responses clearly differed (Fig. 1d, Supplementary Fig. 1a–d), we could directly test the two effector-processing hypotheses (Fig. 1b, c). If the common-processing hypothesis were true, then a processing function (Fig. 1c; $f(x)$) deduced from data from HT-29 cells should accurately predict how activation events in HeLa cells are translated into HeLa-cell-specific apoptosis. Failure of such a model would argue that additional transducer pathways needed to be measured or that cell-specific processing was required (Fig. 1b).

We calculated the effector-processing function by using partial least squares regression (PLSR), a data-driven modelling approach that can connect cell outcomes to network activation[8,20]. We constructed a PLSR model from the dynamic kinase-activation profiles of the seven HT-29 treatment conditions shown in Fig. 1d (see Methods) and the corresponding apoptotic responses 24 and 48 h after TNF stimulation (Supplementary Fig. 1a, c). When the

resulting model was then used *a priori* to predict apoptosis in HeLa cells, we found that the model predictions captured experimental values to within 92% (Fig. 1e). The remarkable accuracy of the HT-29 model for predicting HeLa-specific responses indicated that these two cell types might share a common effector-processing mechanism that converts network activation to apoptosis (Fig. 1c).

To exclude the possibility that common effector processing was unique to transformed cells, we used MCF-10A cells, an immortalized but non-transformed mammary epithelial cell line. Analysis of cell-cycle profiles for HT-29, HeLa and MCF-10A cells revealed that there were similar percentages of cells in G_1, S and G_2/M phase but indicated that the transformed lines carry $2N+$ DNA content owing to chromosomal aberrations (Supplementary Fig. 3a, Supplementary Table 2). Importantly, MCF-10A cells were highly resistant to apoptosis induced by treatment with Adv and TNF compared with HT-29 and HeLa cells (Supplementary Figs 1c, d, 3b), despite being responsive to TNF and readily infected by Adv (Supplementary Fig. 3c, d). To test whether the common effector-processing model could be extended to this third pattern of cell-specific apoptosis, we first stimulated MCF-10A cells with TNF and Adv plus TNF and measured the full time course of kinase activities. As expected, the signalling patterns stimulated by the two treatment combinations in MCF-10A cells were substantially different from those in the transformed lines (Fig. 1d). When the MCF-10A signalling data were input into the common effector-processing model, we found that the resistance of MCF-10A cells to apoptosis induced by treatment with Adv and TNF was correctly predicted within the confidence of the model and the data (Fig. 1e, Supplementary Fig. 4a). Thus, predictions of apoptosis by the common effector-processing model are not limited to transformed cells and might apply to epithelial cells in general.

The kinase activities that we measured are involved in many cellular phenotypes besides apoptosis. If common effector processing is a valid cell-biological principle, then similar models should be trainable for other cell-specific responses. We tested this idea by examining secretion of RANTES (also known as CCL5), a chemokine that is potently induced by both TNF[21] and infection with Adv[22]. The upstream promoter region of RANTES contains putative binding sites for several transcription factors that are direct substrates of the measured kinases[21]. Furthermore, we found that Adv significantly increased TNF-induced secretion of RANTES in HeLa and MCF-10A cells, but not in HT-29 cells (Supplementary Fig. 5). This cell-specific pattern of RANTES secretion was unlike that of apoptosis (Supplementary Figs 1a–d, 3b), indicating that the upstream signal processing was also distinct. Secretion of RANTES induced by treatment with Adv plus TNF therefore provided a cell-specific response that was plausibly controlled by the measured kinases but uncoupled from apoptosis.

We constructed and tested a new chemokine-secretion model by quantifying RANTES in the medium of HT-29, HeLa and MCF-10A cells, 12 and 24 h after treatment with the virus-cytokine combinations used earlier (Fig. 1d). We found that the HT-29 chemokine-secretion model accurately predicted cell-specific RANTES release for the three epithelial lines across five decades (Fig. 1f). HeLa and MCF-10A predictions were accurate to within 88% and 75%, respectively, with considerable overlap in the data-model confidence limits (Supplementary Fig. 4b). Thus, common effector processing applies to multiple cell-specific biological responses.

We next sought to determine whether any cell-specific insight could be gleaned directly from the common effector-processing function of the apoptosis model. The PLSR method derives a set of 'principal components', which contain linear combinations of the original kinase-activity measurements that are optimized to predict outcomes, such as apoptosis[20]. We assigned biological functions to the leading pair of principal components by looking at the projections of HT-29 cells treated with IFN-γ plus TNF. Compared to IFN-γ alone, the IFN-γ plus TNF conditions projected exclusively along

principal component 2 in a dose-dependent manner (Fig. 2a), indicating that principal component 2 was the axis of apoptotic synergy[8]. Compared to TNF alone, the IFN-γ plus TNF treatment also caused a decreased projection along principal component 1, which implied that this orthogonal axis reflected IFN-inducible responses that were unrelated to apoptosis. Consistent with this idea, we found that treatment with Adv (which does not cause apoptosis by itself but activates the type-I IFN response; see below) caused similar projections to treatment with IFN-γ. Consequently, we proposed that responsiveness to Adv–TNF treatment could be broken down into two parts that align with the principal components: an IFN response and an apoptotic response.

We quantified the relative proportions of the IFN and apoptotic responses by comparing the projections arising from treatment with TNF and Adv plus TNF for each cell type along the two principal component axes (Fig. 2b; Supplementary Fig. 6a). HeLa cells projected most strongly along the apoptosis axis, whereas MCF-10A cells had the greatest relative trajectory along the IFN axis, and HT-29 cells had roughly equal responses along both axes. The cell-specific projection along the apoptosis axis correlated with sensitivity to apoptosis induced by treatment with Adv plus TNF (Supplementary Figs 1c, d, 3b). To test the prediction of cell-specific IFN responses, we measured upregulation of the type-I *Ifna* and *Ifnb* genes, along with five IFN-induced genes that have been mechanistically implicated in the antiviral response[23] (Fig. 2c and Supplementary Fig. 6b). All three cell lines showed some induction of IFN expression in response to treatment with Adv, TNF or both. However, MCF-10A cells

showed the most robust IFN response under conditions of Adv–TNF synergy, whereas HeLa cells showed the weakest IFN induction overall and completely lacked Adv–TNF synergy. Therefore, in addition to capturing cell-specific apoptotic responses, the common-processing model revealed an underlying cell-specific responsiveness along the IFN pathway.

An urgent application of common effector processing is to predict cell-specific responses to rational drug therapies[24]. We therefore tested whether the common-processing model could distinguish apoptotic outcomes between tumour cell types (HT-29 and HeLa) when kinase activities were perturbed by inhibitors. The phosphatidylinositol-3-OH kinase (PI(3)K)–Akt/PKB pathway is a clinically relevant cancer target[25] whose inhibition in Adv-infected HT-29 cells markedly increases TNF-induced cell death[11]. However, the role of PI(3)K–Akt signalling in TNF-induced apoptosis of Adv-infected HeLa cells has been unknown.

To predict the effects of inhibition of PI(3)K on HeLa cell viability, we updated the model with measured values[11] of Akt inhibition and apoptosis in HT-29 cells treated with the PI(3)K inhibitor LY294002. We assumed that the potency of LY294002 was constant throughout the 24 h after TNF addition and that no other kinases were affected (see Methods). Next, we experimentally measured the extent to which LY294002 reduced Akt activity in HeLa cells (Fig. 3a). Combining the LY294002-inhibited Akt activity with the corresponding HeLa-network measurements (Fig. 1d), we then used the updated model to predict the response to inhibition of the PI(3)K–Akt pathway when HeLa cells were treated with Adv plus TNF. Surprisingly, the updated model predicted no significant increase
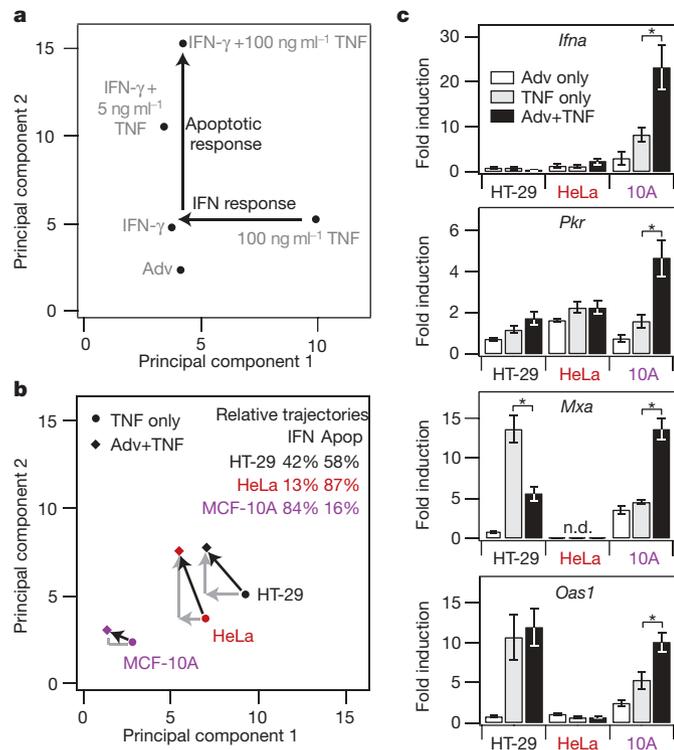

Figure 2 | Principal components of the common-processing model reveal cell-specific IFN responses to treatment with Adv plus TNF. a, b, Reduced principal component dimensions of the common-processing model for HT-29 cells treated with IFN-γ, Adv and TNF (**a**); and HT-29 (black), HeLa (red) and MCF-10A (purple) cells treated with TNF alone (circles) or Adv+TNF (diamonds) (**b**). Protein-kinase signals for each component are included in Supplementary Tables 3 and 4. Apop, apoptosis. **c,** Measurements of IFN-gene induction across cell types. HT-29, HeLa and MCF-10A cells were treated as indicated and collected 16 h later. Experimental data are presented as the mean ± s.e. (n = 3). *Pkr*, gene for double-stranded RNA-dependent protein kinase; *Mxa*, gene for Mx protein GTPase; *Oas1*, gene for 2′,5′-oligoadenylate synthetase 1.
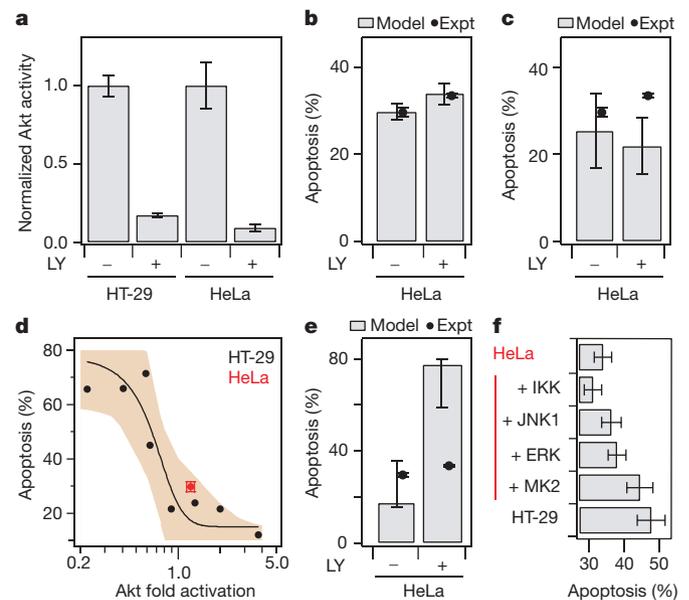

Figure 3 | Common effector processing uniquely predicts resistance of Adv-infected HeLa cells to PI(3)K inhibition. a, Akt activity measured in Adv-infected HT-29 cells and HeLa cells 12 h after TNF stimulation with or without 20 μM LY294002 (LY). Experimental data are presented as the mean ± s.e. (n = 6 for HT-29, n = 6 for HeLa). **b, c,** Apoptosis predicted by the common-processing model (**b**) or HeLa cell-specific processing model (**c**) compared with that measured experimentally (expt) in HeLa cells treated with Adv plus TNF with or without 20 μM LY. **d,** One-kinase relationship linking Akt activity to apoptosis of HT-29 cells (black) treated with combinations of IFN-γ, Adv, and TNF[11] and HeLa cells (red) treated with 100 MOI Adv and 100 ng ml⁻¹ TNF. 95% confidence interval (tan) is shown. **e,** Apoptosis predicted by the Akt-apoptosis model and measured experimentally (markers) in HeLa cells treated with Adv plus TNF with or without 20 μM LY. **f,** Apoptosis predicted by the common-processing model for HT-29–HeLa hybrid-cell profiles containing mixtures of HT-29 signals (black) and HeLa signals (red). Experimental data are presented as the mean ± s.e. (n = 3), and model uncertainties are estimated by jack-knifing[30].

in apoptosis in HeLa cells treated with Adv plus TNF after inhibition of PI(3)K activity, which we confirmed by direct measurement in PI(3)K-inhibited HeLa cells (Fig. 3b and Supplementary Fig. 7). Thus, both the model and experiment indicate that the role of PI(3)K in apoptosis induced by treatment with Adv plus TNF is cell specific: apoptosis of HT-29 cells is PI(3)K-sensitive[11], whereas apoptosis of HeLa cells is PI(3)K-resistant.

The accurate LY294002 predictions in HeLa cells provided us with the opportunity to compare the common model directly against competing mechanisms of effector processing. To mimic cell-specific processing (Fig. 1b), we trained a separate function based only on HeLa measurements and tested whether the existing HeLa data were superior for correctly relating signals to apoptosis. With the relatively few observations, the HeLa-specific model was highly uncertain and far less accurate than the common-processing model based on HT-29 data (Fig. 3c). This emphasized that HT-29-specific information, and thus common effector processing, was essential for prediction using the present data set.

A reductionist alternative to common effector processing is that there exists one crucial transducer, which is a master regulator of Adv–TNF synergy across cell types. TNF-induced apoptosis is highly dependent on the relative extent of Akt activation[11,26], and Akt activation 12 h after treatment predicted apoptosis in Adv-infected HeLa cells (Fig. 3d). This raised the possibility that Akt signalling alone was sufficient to predict cell-specific apoptosis. However, when the Akt model was used with LY294002-inhibited measurements, it incorrectly predicted a fourfold increase in apoptosis in HeLa cells treated with Adv plus TNF (Fig. 3e), indicating the need for signalling information from multiple pathways. This requirement was investigated further by individually substituting HT-29-cell kinase-activity time courses into the LY294002-inhibited HeLa cell data set to construct hybrid-cell profiles (see Methods). In the common-processing model, no one kinase was dominant (Fig. 3f), in agreement with the distributed information provided by these pathways (Supplementary Fig. 8). Among the competing mechanisms for achieving cell specificity, we conclude that common effector processing is most consistent with the experimental data.

The IKK–NF-κB pathway is another important drug target for treating both cancer and inflammatory diseases[27]. However, the value of IKK or NF-κB inhibitors has been debated because the pathway operates very differently across cell types[5]. We used the common-processing model to predict how inhibition of the IKK–NF-κB pathway by SC-514 would affect apoptosis in HT-29 and HeLa cells. We measured the extent to which SC-514 inhibited IκBα degradation in HT-29 and HeLa cells (Supplementary Fig. 9) and then simulated IKK inhibition as described for Akt (see Methods).

Given the new SC-514 signalling inputs, the common-processing model predicted that pretreatment of HT-29 cells with SC-514 would negligibly affect apoptosis (Fig. 4a upper; conditions 1–4), which almost exactly matched the measured values (Fig. 4a upper; conditions 5–8). By contrast, apoptosis of HeLa cells was predicted to increase substantially in uninfected cells treated with SC-514 (Fig. 4a lower; conditions 1–2) and to decrease slightly in Adv-infected cells (Fig. 4a lower; conditions 3–4). Validation experiments showed that the model roughly captured the SC-514-mediated increase in TNF-induced apoptosis of uninfected HeLa cells (Fig. 4a lower; conditions 1–2 and 5–6) but incorrectly predicted apoptosis after SC-514 inhibition in Adv-infected HeLa cells (Fig. 4a lower; conditions 3–4 and 7–8). We found the same pattern of cell-specific apoptosis when using two other small-molecule inhibitors that target different points on the IKK–NF-κB pathway (Supplementary Fig. 10). Thus, the common-processing model had qualitatively predicted the existence of cell-specific responses to inhibition of the IKK–NF-κB pathway, but did not quantitatively predict the extent of specificity in HeLa cells treated with Adv plus TNF.

The discrepancy between the model and the experimental data was not necessarily due to failure of common processing but instead

could arise from limitations in the HT-29 data that were used to train the PLSR model[20]. We compared the distribution of IKK measurements in HeLa cells with the HT-29 training data and found that the data for treatment with Adv plus TNF contained several IKK-activity observations that were higher than any previously measured in HT-29 cells (Supplementary Fig. 11). Furthermore, all of these very high IKK activities occurred within 4 h of TNF treatment (Fig. 4b), when IKK activity is considered to be anti-apoptotic[8,27]. These observations indicated that the HT-29 training set was not diverse enough to quantify the common-effector relationship between early IKK activity and apoptosis. Predictions of HeLa apoptosis when IKK was inhibited would therefore be uncertain.

An important corollary to this explanation is that early IKK activity should have a disproportionately anti-apoptotic role in HeLa cells. We tested this by performing timed-inhibition experiments with SC-514. Direct inhibition of early IKK signalling was not feasible, because removal of SC-514 caused hyperactivation of IKK (Supplementary Fig. 12). Therefore, we selectively inhibited IKK from 4 h to 24 h and compared the increase in apoptosis to when IKK was inhibited from 0 h to 24 h (Fig. 4c). In HT-29 cells, IKK inhibition from 4 h to 24 h had the same effect as inhibiting IKK from 0 h to 24 h. By contrast, nearly half of the SC-514-mediated increase in HeLa-cell apoptosis could be attributed to early-phase inhibition of IKK (Fig. 4c and Supplementary Fig. 13). Early IKK activation therefore appears to be specifically crucial for anti-apoptotic signalling in Adv-infected HeLa cells. Together, these data support common effector processing as part of the mechanism for achieving cell-specific sensitivity to pharmacological inhibitors and apoptotic stimuli.

Our study reveals an underlying similarity among disparate cell types that becomes evident when signalling information is processed at the network level. Most of the kinases measured here lie at the 'waist' of hourglass-shaped pathways[28], indicating a unique point of convergence in the network architecture (Fig. 1a) that can be exploited to make predictions broadly and accurately. The predictions of cell-specific apoptosis, chemokine secretion, IFN induction and drug sensitivity were focused on epithelial cells for the sake of feasibility. There probably does not exist a common-processing
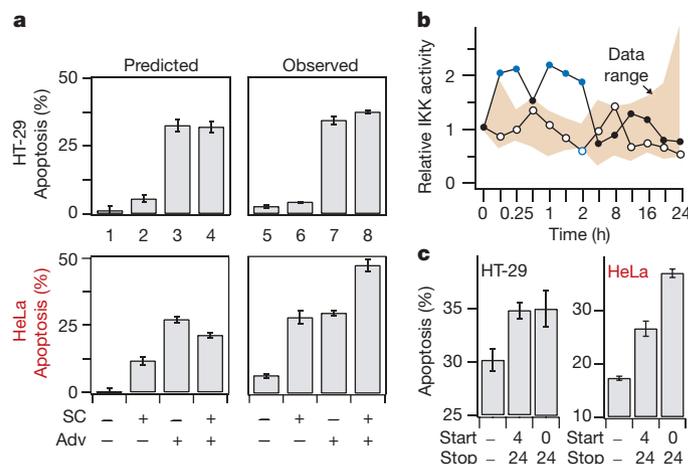

Figure 4 | Deduction of cell-specific sensitivity to early-phase IKK inhibition. a, Apoptosis predicted by the common-processing model (left) and measured experimentally (right) in HT-29 (top) and HeLa (bottom) cells treated with 100 ng ml^{-1} TNF with or without 20 μM SC-514 (SC) and 100 MOI (HeLa) or 1,000 MOI (HT-29) Adv pre-infection. **b,** Range plot of HT-29 IKK activity used for model training (tan) and IKK activity time course of HeLa cells treated with TNF (open) or Adv plus TNF (filled). Points outside the training range are highlighted in blue. **c,** TNF-induced apoptosis in Adv-infected HT-29 and HeLa cells following IKK inhibition with 20 μM SC-514 for the indicated times. Data are presented as the mean ± s.e. ($n = 3$), and model uncertainties are estimated by jack-knifing[30].

function that captures responses across all cell types. Consistent with this expectation, our preliminary attempts to extend a reduced version of the common effector-processing model to apoptosis of Jurkat cells (a leukaemic T-cell line) led to highly uncertain predictions (Supplementary Fig. 14). Nonetheless, for a diverse range of epithelia, our data support the existence of common effector mechanisms that can predict cell fate. Such mechanisms are revealed only after applying a data-driven modelling approach that converts important kinase-signalling events into a phenotype[8,20].

If the common-processing hypothesis had failed, it would have meant that each cell type would require its own in-depth experiments and model training. Our results raise the possibility that models can be refined with new data to the point that they enable accurate predictions of phenotype that are broadly applicable. Already, the distinction between two carcinoma lines on the basis of their apoptotic response to PI(3)K and IKK inhibition points towards immediate applications for combining pharmacological inhibitors[6] and cancer gene therapy[7] to treat certain tumours.

METHODS SUMMARY

HT-29 cells, HeLa cells (American Type Culture Collection) and MCF-10A cells were grown as described[11,29]. Infection with Adv, stimulation with TNF, pre-treatment with IFN-γ and lysis were performed essentially as described[11,18]. Small molecule inhibitors (Calbiochem) were spiked into media 1–2 h before TNF stimulation. Kinase activities were measured by a microtitre-based assay[26] and were confirmed to operate in the linear range for each cell type (Supplementary Fig. 15). Values are normalized to the 0-min time point and then multiplied by cell-specific and kinase-specific correction factors (Supplementary Table 5). Descriptors of signalling dynamics were derived as described elsewhere[8]. Network-activation time courses were concatenated, log transformed, and normalized to the maximum observed value for each kinase. Clustering was performed by the unweighted pair group method with arithmetic mean and a Euclidean distance metric. Apoptosis was measured by flow cytometry for cleaved caspase-cytokeratin as described[11]. For RANTES secretion, we collected supernatants and analysed them according to the manufacturer's recommendations (R&D Systems). Gene induction was measured by real-time quantitative PCR on a LightCycler II instrument (Roche) with standard curves based on purified amplicons. The PLSR model was constructed using SIMCA-P (Umetrics) as described[8]. Model calibrations were made by leave-one-out cross-validation[19] for the HT-29 treatments, and model uncertainties were calculated by jack-knifing[30]. For inhibitor predictions, the target kinase activity was held constant at the experimentally measured inhibited value, time-course activities of the other kinases were kept the same as before, and signalling descriptors were recalculated. We used Student's t-test to compare two individual means, and two-factor ANOVA to compare two activity time courses. We calculated nonlinear confidence intervals by support plane analysis.

Full Methods and any associated references are available in the online version of the paper at www.nature.com/nature.

1. Gerhart, J. 1998 Warkany lecture: signaling pathways in development. *Teratology* **60**, 226–239 (1999).
2. Jordan, J. D., Landau, E. M. & Iyengar, R. Signaling networks: the origins of cellular multitasking. *Cell* **103**, 193–200 (2000).
3. Downward, J. The ins and outs of signalling. *Nature* **411**, 759–762 (2001).
4. Irish, J. M. *et al.* Single cell profiling of potentiated phospho-protein networks in cancer cells. *Cell* **118**, 217–228 (2004).
5. Wajant, H., Pfizenmaier, K. & Scheurich, P. Tumor necrosis factor signaling. *Cell Death Differ.* **10**, 45–65 (2003).
6. Kenakin, T. Predicting therapeutic value in the lead optimization phase of drug discovery. *Nature Rev. Drug Discov.* **2**, 429–438 (2003).
7. McCormick, F. Cancer gene therapy: fringe or cutting edge? *Nature Rev. Cancer* **1**, 130–141 (2001).
8. Janes, K. A. *et al.* A systems model of signaling identifies a molecular basis set for cytokine-induced apoptosis. *Science* **310**, 1646–1653 (2005).
9. Schmitz, E. K., Kraus, D. M. & Bulla, G. A. Tissue-specificity of apoptosis in hepatoma-derived cell lines. *Apoptosis* **9**, 369–375 (2004).
10. Ohmori, Y. & Hamilton, T. A. Cell type and stimulus specific regulation of chemokine gene expression. *Biochem. Biophys. Res. Commun.* **198**, 590–596 (1994).
11. Miller-Jensen, K., Janes, K. A., Wong, Y. L., Griffith, L. G. & Lauffenburger, D. A. Adenoviral vector saturates Akt pro-survival signaling and blocks insulin-mediated rescue of tumor necrosis-factor-induced apoptosis. *J. Cell Sci.* **119**, 3788–3798 (2006).
12. Pawson, T. Specificity in signal transduction: from phosphotyrosine-sh2 domain interactions to complex cellular systems. *Cell* **116**, 191–203 (2004).
13. Bouwmeester, T. *et al.* A physical and functional map of the human TNF-α/NF-κB signal transduction pathway. *Nature Cell Biol.* **6**, 97–105 (2004).
14. Cho, K. H., Shin, S. Y., Lee, H. W. & Wolkenhauer, O. Investigations into the analysis and modeling of the TNFα-mediated NF-κB-signaling pathway. *Genome Res.* **13**, 2413–2422 (2003).
15. Janes, K. A. & Lauffenburger, D. A. A biological approach to computational models of proteomic networks. *Curr. Opin. Chem. Biol.* **10**, 73–80 (2006).
16. Philpott, N. J., Nociari, M., Elkon, K. B. & Falck-Pedersen, E. Adenovirus-induced maturation of dendritic cells through a PI3 kinase-mediated TNF-alpha induction pathway. *Proc. Natl Acad. Sci. USA* **101**, 6200–6205 (2004).
17. Liu, T. C. *et al.* Functional interactions of antiapoptotic proteins and tumor necrosis factor in the context of a replication-competent adenovirus. *Gene Ther.* **12**, 1333–1346 (2005).
18. Janes, K. A. *et al.* The response of human epithelial cells to TNF involves an inducible autocrine cascade. *Cell* **124**, 1225–1239 (2006).
19. Gaudet, S. *et al.* A compendium of signals and responses triggered by prodeath and prosurvival cytokines. *Mol. Cell. Proteomics* **4**, 1569–1590 (2005).
20. Janes, K. A. & Yaffe, M. B. Data-driven modelling of signal-transduction networks. *Nature Rev. Mol. Cell Biol.* **7**, 820–828 (2006).
21. Nelson, P. J., Kim, H., Manning, W., Goralski, T. & Krensky, A. Genomic organization and transcriptional regulation of the RANTES chemokine gene. *J. Immunol.* **151**, 2601–2612 (1993).
22. Bowen, G. P. *et al.* Adenovirus vector-induced inflammation: capsid-dependent induction of the C–C chemokine RANTES requires NF-κB. *Hum. Gene Ther.* **13**, 367–379 (2002).
23. Samuel, C. E. Antiviral actions of interferons. *Clin. Microbiol. Rev.* **14**, 778–809 (2001).
24. Dancey, J. & Sausville, E. A. Issues and progress with protein kinase inhibitors for cancer treatment. *Nature Rev. Drug Discov.* **2**, 296–313 (2003).
25. Luo, J., Manning, B. D. & Cantley, L. C. Targeting the PI3K-Akt pathway in human cancer: rationale and promise. *Cancer Cell* **4**, 257–262 (2003).
26. Janes, K. A. *et al.* A high-throughput quantitative multiplex kinase assay for monitoring information flow in signaling networks: application to sepsis-apoptosis. *Mol. Cell. Proteomics* **2**, 463–473 (2003).
27. Karin, M. & Greten, F. R. NF-κB: linking inflammation and immunity to cancer development and progression. *Nature Rev. Immunol.* **5**, 749–759 (2005).
28. Csete, M. & Doyle, J. Bow ties, metabolism and disease. *Trends Biotechnol.* **22**, 446–450 (2004).
29. Debnath, J., Muthuswamy, S. K. & Brugge, J. S. Morphogenesis and oncogenesis of MCF-10A mammary epithelial acini grown in three-dimensional basement membrane cultures. *Methods* **30**, 256–268 (2003).
30. Janes, K. A. *et al.* Cue-signal-response analysis of TNF-induced apoptosis by partial least squares regression of dynamic multivariate data. *J. Comput. Biol.* **11**, 544–561 (2004).

METHODS

Adenoviral vectors. The recombinant adenovirus type 5 vectors were deleted for E1 and E3 regions and expressed *Escherichia coli* β-galactosidase (β-gal) under control of the cytomegalovirus (CMV) enhancer/promoter (provided by the University of Michigan Vector Core). Virus was reported to have an infectious plaque-forming unit (p.f.u.) concentration of 1 p.f.u. for every 23.5 viral particles (v.p.) as determined by plaque assay.

Cell culture and stimulation. HT-29 and HeLa cells were grown according to ATCC recommendations and plated at 50,000 and 20,000 cells per cm^2, respectively. The cell densities for HT-29 and HeLa cells were optimized to have approximately the same number of cells at the end of the standardized 4-day experimental protocol. MCF-10A cells were grown as described[29] and plated at a density of 50,000 cells per cm^2. HT-29 cells were infected with 0, 1.4×10^9 or 1.4×10^{10} v.p. ml^{-1} Adv (0, 100 or 1,000 MOI), HeLa cells with 0 or 7.4×10^8 v.p. ml^{-1} Adv (0 or 100 MOI), and MCF-10A cells with 0 or 1.4×10^9 v.p. ml^{-1} Adv (0 or 100 MOI). Infections were performed essentially as described[11]. The infection MOI for HT-29 and HeLa cells was chosen to maximize the difference in cell response according to published Adv dose responses in the presence of 100 ng ml^{-1} TNF[11]. Cells pretreated with IFN-γ were prepared and lysed as described[18]. Twenty-four hours after the start of infection, cells were spiked with 100 ng ml^{-1} TNF (Peprotech) for 5, 15, 30, 60 and 90 min and 2, 4, 8, 12, 16, 20 and 24 h and lysed as described[11,26]. For Akt perturbation, LY294002 or wortmannin (Calbiochem) was spiked into the medium 1 h before TNF stimulation. For IKK–NF-κB pathway perturbation, SC-514, SN-50, or BAY 11-1082 (Calbiochem) was spiked into the medium 2 h before TNF stimulation. For small-molecule inhibitor controls, the carrier alone (0.02–0.1% DMSO) or SN50M (control peptide for SN50) was added.

Network-level signalling measurements. Kinase activities for five network signals—ERK, Akt, JNK1, IKK and MK2—were quantitatively measured by a microtitre-based assay[26]. All kinase assays were confirmed to operate in the linear range for each cell type (Supplementary Fig. 15). Values are presented as the mean of duplicate biological samples, normalized to the 0-min time point from quadruplicate biological samples. To adjust for cell-specific differences in basal activities, kinase-specific correction factors were calculated for each cell type by scaling the median 0-min (untreated) activity values (Supplementary Table 5) to the 0-min activity of the kinase in HT-29 cells (assigned a nominal value of 1). The fold activations of HeLa and MCF-10A cells were then multiplied by the cell- and kinase-specific correction factors to fuse the data sets for the PLSR-model predictions. The final processed data were normalized to the maximum value of each signal across all conditions to aid comparison of signals with different dynamic ranges. Descriptors of signalling dynamics were derived for each time course as described[8].

Apoptosis measurements. Cells that scored double-positive for cleaved cytokeratin (a caspase-3/6/7 substrate) and cleaved-caspase-3 were measured by flow cytometry as described[11].

Enzyme-linked immunosorbant assay. HT-29, HeLa and MCF-10A cells were treated in parallel according to the conditions described in Fig. 1d. Supernatants were collected after 12 and 24 h and analysed for RANTES secretion according to the manufacturer's recommendations (R&D Systems). Receptors for RANTES are not detectable in HT-29[31], HeLa[32] and MCF-10A cells (K.A.J. and J.S.B., unpublished observations), which avoids the confounding effects of autocrine binding in these cells. Measurements were normalized to live-cell counts collected in parallel with the supernatants after 12 and 24 h. To account for different basal levels of secretion across cell types, the HT-29 secretion data were mean-centred and variance-scaled before training the PLSR model. The predicted TNF-induced RANTES secretion in HeLa and MCF-10A cells were transformed back to absolute physical units based on the mean and variance of observed HeLa and MCF-10A RANTES secretion data across four conditions (no treatment, TNF only, Adv plus TNF, and IFN-γ plus TNF).

Real-time quantitative PCR (RT-qPCR). HT-29, HeLa and MCF-10A cells were seeded in 12-well plates and treated with Adv and TNF as described. Sixteen hours after TNF stimulation, RNA was prepared by lysing in 0.5 ml RNA STAT-60 (Tel-Test). After phenol-chloroform purification, residual genomic DNA was eliminated with DNA-free (Ambion). First-strand synthesis was performed with 5 μg DNA-free RNA, Superscript III (Invitrogen), and oligo(dT)24 according to the manufacturer's recommendations. RT-qPCR was done using 0.1 μl cDNA template and 10 pmol forward and reverse primers together with a homemade master mix used at a final concentration of $1 \times$ PCR Buffer II (Applied Biosystems), 4 mM MgCl$_2$, 200 μM each of dATP, dCTP, dGTP and dTTP, 150 μg ml^{-1} BSA, 5% glycerol, $0.25 \times$ SYBR green (Invitrogen), and 0.025 U ml^{-1} AmpliTaq (Applied Biosystems) in a final reaction volume of 15 μl. Real-time reactions were tracked on a LightCycler II instrument (Roche) with the following amplification scheme: a denaturation step of 95 °C for 90 s; an amplification step of 95 °C for 10 s, 60 °C for 10 s, 72 °C for 12 s repeated 40 times; a fusion step of 65 °C to 95 °C touched up at 0.1 °C s^{-1}. All primers gave single peaks upon melting-curve analysis (sequences are listed in Supplementary Table 6). Relative levels were determined on the basis of a standard curve of gene-specific amplicons diluted through five orders of magnitude. Samples were normalized to the geometric mean of three housekeeping genes: glyceraldehyde-3-dehydrogenase (*gapdh*), peroxiredoxin 6 (*prdx6*) and histidine triad nucleotide binding protein 1 (*hint1*) (Supplementary Table 6)[33]. Fold induction was calculated for each cell type by normalizing to its own mock-stimulation levels.

Hierarchical clustering. Network-activation time courses were concatenated, log transformed, and normalized to the maximum observed value for each kinase. Clustering was performed by the unweighted pair group method with arithmetic mean and a Euclidean distance metric.

PLSR model construction and refinement. The PLSR model was constructed using SIMCA-P (Umetrics) as described[8]. The predictive power of the HT-29 model was calculated by leave-one-out cross-validation[19] (73% predictive power for apoptosis model and 81% for RANTES secretion). Model uncertainties were calculated by jack-knifing[30]. Treatment projections were plotted after a 109° subspace rotation of the principal component vectors. To approximate the dynamic network behaviour for a given treatment in the presence of PI(3)K inhibition, we held the level of Akt constant at the LY294002-inhibited activity fraction measured after 12 h (Fig. 3a) for HT-29 (0.17) and HeLa (0.09) compared to a 0-min baseline. Similarly, IKK activity levels were held constant at the measured SC-514-inhibited activity fraction (Supplementary Fig. 8; 0.65 for HT-29; 0.48 for HeLa). With both inhibitor predictions, time-course values of the other kinases were kept identical to the network behaviour measured in the absence of inhibitor, and metrics were extracted as described above. For HT-29–HeLa cell hybrid profiles, the measured HeLa kinase activities from Adv–TNF treatment were replaced one at a time with the corresponding kinase activities measured in HT-29 cells, and metrics were extracted as described above.

Statistical analysis. We used Student's *t*-test to compare two means, and two-factor ANOVA to compare two activity time courses. All tests were performed at a significance level of α = 0.05. Nonlinear confidence intervals were calculated by support plane analysis[34].

31. Jordan, N. J. *et al.* Expression of functional CXCR4 chemokine receptors on human colonic epithelial cells. *J. Clin. Invest.* **104**, 1061–1069 (1999).
32. Choe, H. *et al.* The beta-chemokine receptors CCR3 and CCR5 facilitate infection by primary HIV-1 isolates. *Cell* **85**, 1135–1148 (1996).
33. Vandesompele, J. *et al.* Accurate normalization of real-time quantitative RT-PCR data by geometric averaging of multiple internal control genes. *Genome Biol.* **3**, research0034.1–0034.11 (2002).
34. Lakowicz, J. R. *Principles of Fluorescence Spectroscopy* 2nd edn 118–124 (Kluwer Academic/Plenum, New York, 1999).